Characterization of naturally-occurring particles in the NASA Langley 0.3-m Transonic Cryogenic Tunnel using PTV

Ross A. Burns[1] and Jian Gao[2]
ViGYAN, Inc., Hampton, VA, 23666, USA

Paul M. Danehy[3]
NASA Langley Research Center, Hampton, VA, 23681, USA

Naturally-occurring particles within the NASA Langley 0.3-m Transonic Cryogenic Tunnel are characterized for their aerodynamic performance using particle tracking velocimetry. Two sets of experiments were conducted to observe different behaviors of the particles. The normal shockwave emanating from the top surface of a supercritical airfoil was used to induce velocity lag in the particles, and the subsequent spatial decay of the velocity was used to estimate the effective diameter of the particles. Mean particle diameters between 1.6 and 1.9 μm were measured, with sizes ranging from 0.2 to 3.5 μm over the entire ensemble. The response of particles to separated flow was investigated. By operating in "high-lift" (low Mach number, high angle of attack) conditions with a semi-span airfoil, the ability of particles to detect separated flow on the upper surface of the airfoil was assessed. Transition from fully attached flow to fully separated flow was observed on the top surface of the airfoil accompanying a variation of angle of attack from 8° to 12°. Examination of velocity distributions indicates less than 10 percent of particle trajectories did not respond to the regions of separated flow. These results are promising, but further facility-specific work is needed to answer the broader question of particle tracking reliability.

I. Introduction

The development and deployment of optical measurements within high-pressure, cryogenic wind tunnels have been advancing in recent years despite mechanical constraints of these systems: limited to no optical access, intense vibrations, frost formation and condensation, size and scale of the facilities, and large density fluctuations in and around the facilities. For example, the first external optical penetration for the National Transonic Facility (NTF) was installed in 2018 [1]. Due to this slow-moving development cycle, any advantage that can be leveraged to accelerate and facilitate further development is welcomed. The femtosecond laser electronic excitation tagging (FLEET) technique, which has been utilized in both the NASA Langley 0.3-m Transonic Cryogenic Tunnel (0.3-m TCT) [2] and the NTF [3], took advantage of the nitrogen flow circuits to successfully make velocity measurements in both tunnel freestreams and more practical environments. One class of techniques that has been forestalled since the inception of these facilities at NASA Langley are particle-based measurements such as particle image velocimetry (PIV) or particle tracking velocimetry (PTV). Though only used sporadically, these techniques have advanced more rapidly in the European TCTs due in part to the introduction of external seed media such as oil and ice crystals [4], but operational protocols at the NASA Langley facilities generally prohibit this pathway to avoid contaminating the flow circuits. However, it has been known for at least 40 years that particles of unclear character are present within the flow circuits of these facilities [5, 6] and persist to this day. Previous researchers have attempted to utilize the

[1] Senior Research Engineer, Advanced Measurement and Data Systems Branch.
[2] Research Engineer, Advanced Measurement and Data Systems Branch.
[3] Senior Technologist, Advanced Measurement and Data Systems Branch, AIAA Associate Fellow.

particles for velocity measurements in these facilities including the use of laser Doppler anemometry [7] and laser transit anemometry [8], but the presence and quality of the seed has been erratic, which may be linked to the ongoing history of the 0.3-m TCT facility [9]. For example, an attempt to measure particle size was made by Hall [10], only to have the particles no longer be present a year later after routine maintenance of the facility [11]. An ongoing uncertainty also exists about the material composition of these particles. It was initially thought that the particles were unevaporated LN2 (liquid nitrogen) [12]. However, the presence of these particles at elevated temperatures suggested that another substance, possibly oil, was also present in the flow circuit [10]. More recent studies have proposed that the particles may result from the desublimation of trace water vapor from the injected liquid nitrogen [13]. Although presently unknown, it is likely that the particles that exist at elevated temperatures are a combination of different substances, while a larger fraction of the particles are comprised of LN2 as the operating temperature of the facility is decreased. It is noted that other facilities have unique challenges surrounding these types of particles in the flow circuit. In the NTF, for example, it is speculated that a fraction of the particles present in the freestream are insulation fibers [6]. For the use of most Mie-scattering-based techniques, however, the aerodynamic properties of these particles are ultimately more important than their composition.

Despite the unknown and possibly changing character of these particles, progress continues to be made toward understanding and utilizing them for measurements. PIV was performed in the freestream of the 0.3-m TCT recently [**Error! Bookmark not defined.**]. While the accuracy of these measurements was noteworthy, attempts at further characterizing these particles or using them for practical measurements have been difficult to implement. Moreover, the ongoing challenges of using the FLEET technique in the NTF have placed more emphasis on the development of particle-based flow diagnostics, since they are generally more robust in harsh environments. In this paper, the first successful attempt to use this passive seeding for PTV in the 0.3-m TCT facility, with models in place, is documented. A method to perform an *in situ* characterization of the particle size is established; PTV is performed across a normal shock generated by a transonic airfoil, and particle size is assessed by fitting particle dynamics simulations to the observed spatial velocity decay. Velocity measurements are then attempted in a region of separated flow generated by a semi-span airfoil under high-lift tunnel conditions to determine both the feasibility and sensitivity of the technique. Details about the experimental setup and results from these studies are presented in this paper, while details about data analysis can be found in the appendix.

II. Experimental Setup

These experiments were divided into two phases. The first phase of testing attempted to measure the observed velocity change across a normal shockwave generated by a transonic airfoil for the purposes of measuring particle lag and subsequently estimating the ensemble mean particle diameter. The second phase of testing examined the flow over an airfoil at high-lift conditions, specifically to determine if observing flow separation associated with high angle-of-attack (AoA) operation was possible with the natural particles. This section discusses the experimental setups used in each of these two testing campaigns.

A. Experimental facility

Both test campaigns were conducted in the 0.3-m Transonic Cryogenic Tunnel (0.3-m TCT) located at NASA Langley Research Center in Hampton, VA. This facility is a fan-driven, closed-loop wind tunnel capable of running with both air and nitrogen as the working fluid, though only nitrogen was used in these experiments. The 0.3-m TCT can operate at total (stagnation) pressures ranging from 100 to 500 kPa and total temperatures from 100 to 325 K. Additionally, the facility operates at Mach numbers ranging from 0.2 to 0.85 in a continuous manner, though there is some flexibility on both ends of this range for short durations. Test article blockage can prevent operation at the highest Mach numbers for some configurations and conditions. For the phase-1 (normal shock) studies, a range of Mach numbers from 0.6 to 0.74 were tested, typically at the highest allowable total design pressures of the model. In the phase-2 studies (high-lift), the Mach number was kept low in the 0.2 - 0.3 range with similarly low operating pressures to emulate the conditions experienced during high-lift operation of an airfoil.

The 0.3-m TCT test section has a double-shelled construction. The inner test section dimensions are 0.33 m × 0.33 m. The test section is surrounded by an outer plenum of nominally quiescent gas. The top and bottom walls of the facility were set to be slightly diverging during these tests to account for the growth of the boundary layers. Optical access for these experiments was varied between the two phases. For the phase-1 testing, a single, circular window allowed the laser and camera to view through the outer pressure shell, while a D-shaped, hexagonal window was present in each of the test section sidewalls. In contrast, the phase-2 tests utilized a single slot-shaped window in the test section sidewall for viewing the airfoil model, while still utilizing the circular window in the outer pressure shell. Note that operation with the slot-shaped window limited the lowest operational temperature to a total temperature

greater than or equal to 200 K as a precaution to avoid window damage. Finally, the coordinate system used in these studies is worth noting; the x-, y-, and z-coordinates all originate at the center of the test section and correspond to the streamwise, transverse, and spanwise directions, respectively.

B. Test articles

The phase-1 (normal shock) tests utilized a supercritical airfoil designated NASA SC(3)-0712(B) [14], which has been used previously for testing pressure sensitive paint [15]. A cross-sectional profile shown in Fig. 1a. This airfoil model was full-span and mounted such that the center of rotation was at the mid-chord position. The model angle of attack (AoA, α) was adjustable by rotation of the turntables embedded in the tunnel sidewalls. Though adjustable through a much larger range, the AoA was only varied between 3° and 5° during testing. Due to the full-span nature of this model, the optical access to the test section was limited to the D-shaped window above the top surface of the airfoil. The phase-2 (high-lift) studies utilized a semi-span, tapered airfoil; the profile can be seen in Fig. 1b. Previous tests of the FLEET technique utilized this airfoil to demonstrate measurement capabilities [16]. In similar fashion to the other airfoil model, the airfoil AoA could be adjusted by rotation of the turntable embedded in the tunnel sidewall. In this case, the AoA ranged from 0° to 20°. The center of rotation was about the trailing edge at the 1/2 span position of the airfoil.

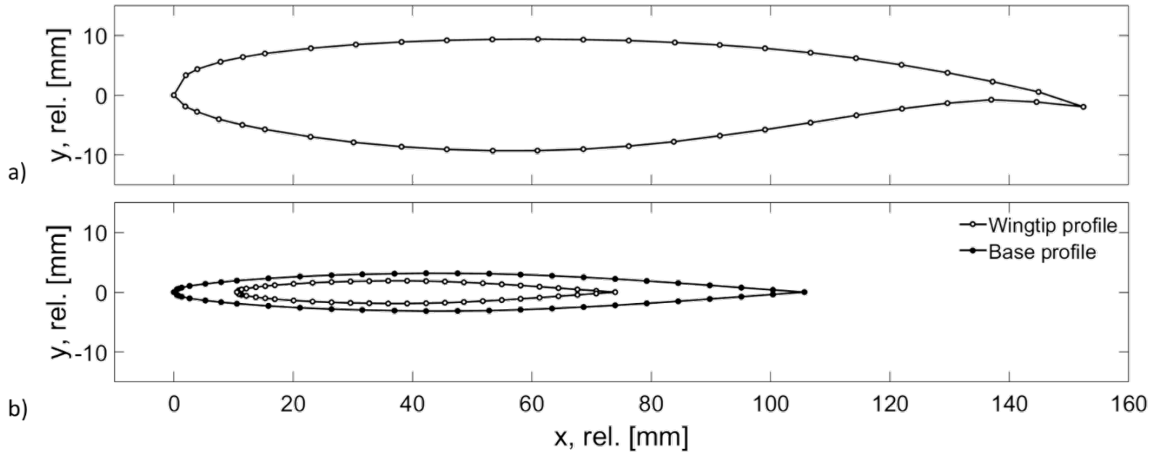

Figure 1. Cross-sectional profiles of the two airfoils used in these experiments. a) Full-span, supercritical airfoil SC(3)-0712(B) and b) semi-span airfoil.

C. Laser and optical systems

The laser used in these studies was a burst-mode, master oscillator, pulsed amplifier system (Spectral Energies QuasiModo 1200[1]). To accommodate different data acquisition modes, the laser operated in either single- or double-pulse modes with repetition rates up to 1 MHz and total burst energies between 40 and 60 J at 532 nm. The laser was paired with a high-speed CMOS camera (Photron Fastcam Nova S20), which is a 10-bit camera able to acquire full-frame images (1024 px × 1024 px) at 18.75 kHz.

1. Phase 1 – Normal Shock

An overview of the experimental setup for the phase 1 studies can be seen in Fig. 2. The output from the laser system was first directed through an external optical attenuator to reduce the overall energy content of the burst without negatively affecting beam quality. The beam was then directed through an astigmatism-correcting telescope to correct a long-distance focusing issue the laser was experiencing at the time. The left panel of Fig. 2 depicts this portion of the setup. The beam was then directed from an upper mezzanine down to the tunnel level – a distance of about 4 meters – by periscope. A series of four cylindrical lenses was used to form the beam into the desired sheet including paired -50-mm and +300-mm in the horizontal direction and +200-mm and -100-mm in the vertical direction. At the

[1] Specific vendor and manufacturer names are explicitly mentioned only to accurately describe the test hardware. The use of vendor and manufacturer names does not imply an endorsement by the U.S. Government nor does it imply that the specified equipment is the best available.

measurement location, the laser sheet was approximately 64 mm wide and 2.5 mm thick. However, the observable area was about 1.5 times this width, since the back-reflection off the second window allowed additional scattering to be observed. Though only a fraction of the laser sheet energy was reflected from this window, the particle scattering was observed as forward scatter, which has higher intensity compared to the back scatter seen from the incident laser sheet. After the sheet-forming lenses, the laser sheet was directed into the tunnel through the circular pressure-shell window, and then through the test section with a periscopic mirror pair before finally being directed to a beam dump on the opposite side of the plenum. The camera, which was equipped with a 135-mm lens (set to $f/8$), viewed scattering from the particles through the D-shaped window by using an imaging periscope within the plenum. Additionally, the lens was Scheimpflug-mounted to the camera to maintain focus at the heavily skewed viewing angle. The overall optical setup in the vicinity of the test section can be seen in the center and right panels of Fig. 2.

For these studies, the pulse-burst laser was operated in double-pulse mode; the primary repetition rate was set to 20 kHz, while the interpulse delay was set to either 2.5 or 5 μs. To accommodate this operation, the camera system was timed to acquire at 40 kHz, frame straddling the double-pulse from the laser system. Approximately 200 valid image pairs were collected for each burst.

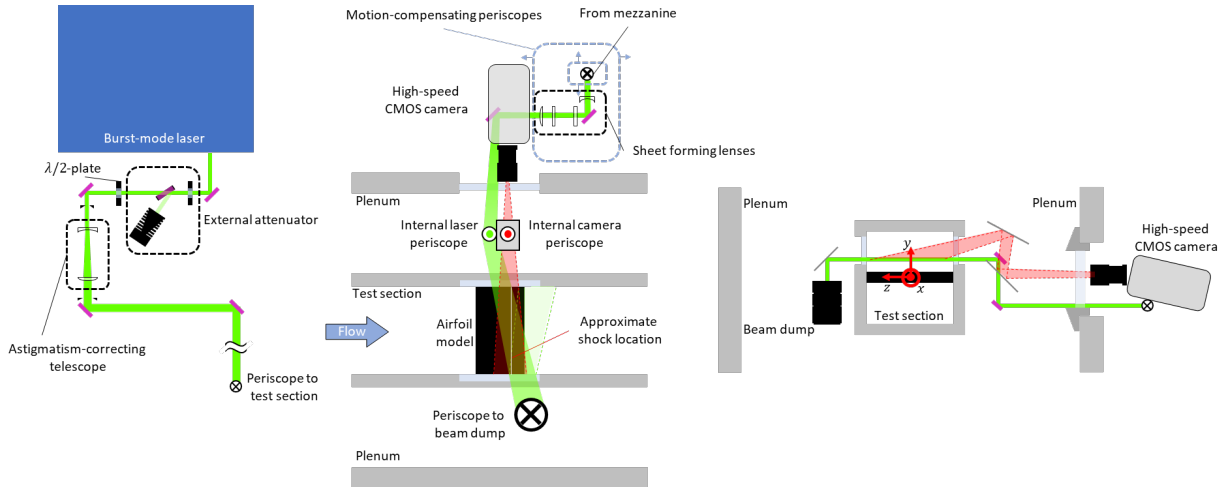

Figure 2. Phase-1 optical setup. Left panel, setup near laser head. Center panel, top view of optical setup in and around test section. Right panel, end view of optical setup inside test section.

2. Phase 2 – High-Lift

The phase-2 studies utilized a slightly less complicated optical system than the previous tests. Figure 3 gives an overview of the optical setup for the phase-2 studies. The beam from the pulse-burst laser was first directed through an external attenuator as described above. The beam was subsequently directed through a short up-periscope to rotate the beam 90°. The laser sheet was formed on the mezzanine in these studies using four cylindrical lenses (paired −37.5-mm and +150-mm in the vertical direction and −150-mm and +300-mm in the horizontal direction). At the measurement location, the sheet was approximately 40 mm (height) × 5 mm (thickness). This optical arrangement is depicted in the left panel of Fig. 3. The laser sheet was directed down to the test section, into the plenum, and then through the test section with a series of mirrors. The laser sheet passed over the airfoil (mounted on the opposite side of the tunnel) at a 55° angle (relative to the streamwise direction) before hitting the far wall. A small amount of divergence was present in the sheet, and it was angled up slightly as it passed over the airfoil to accommodate a larger range of AoA during the test. The camera was again equipped with a 135-mm lens (set to *f*/4) and was positioned to look straight through the test section at the wing model. A scheimpflug mounting scheme was again utilized to compensate for the non-perpendicular laser sheet. The setup around the test section is depicted in the center panel of Fig. 3, while the position of the laser sheet over the surface of the airfoil can be seen in the right panel of the same figure.

For this experiment, the laser was set to operate at 100 kHz, single pulsed for the majority of data acquisition. The camera was accordingly set to frame at 100 kHz, and the central 2/3 of the airfoil was visible within the field-of-view. A time-series of 1000 images was acquired from each burst. Raw data samples from both the phase-1 and phase-2 experiments can be seen in Fig. 4.

D. Miscellaneous

In addition to the optical instrumentation, the 0.3-m TCT facility was equipped with an extensive data acquisition system (DAS), which recorded relevant test conditions during the experiments. This system comprised an array of static and total pressure probes throughout the facility, as well as thermocouple probes and strain gauges. These data were read into a network of facility computer systems for processing and were later used to confirm experimental conditions and validate freestream data when required.

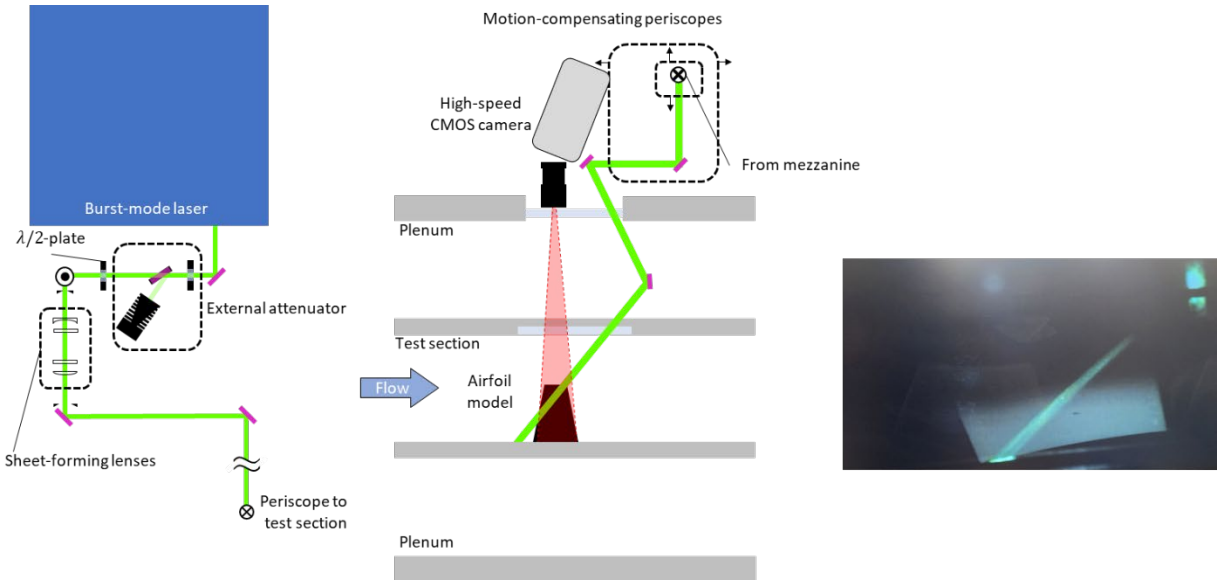

Figure 3. Phase-2 optical setup. Left panel, setup near laser head. Center panel, top view of optical setup in and around test section. Right panel, position of laser sheet passing over the airfoil model.

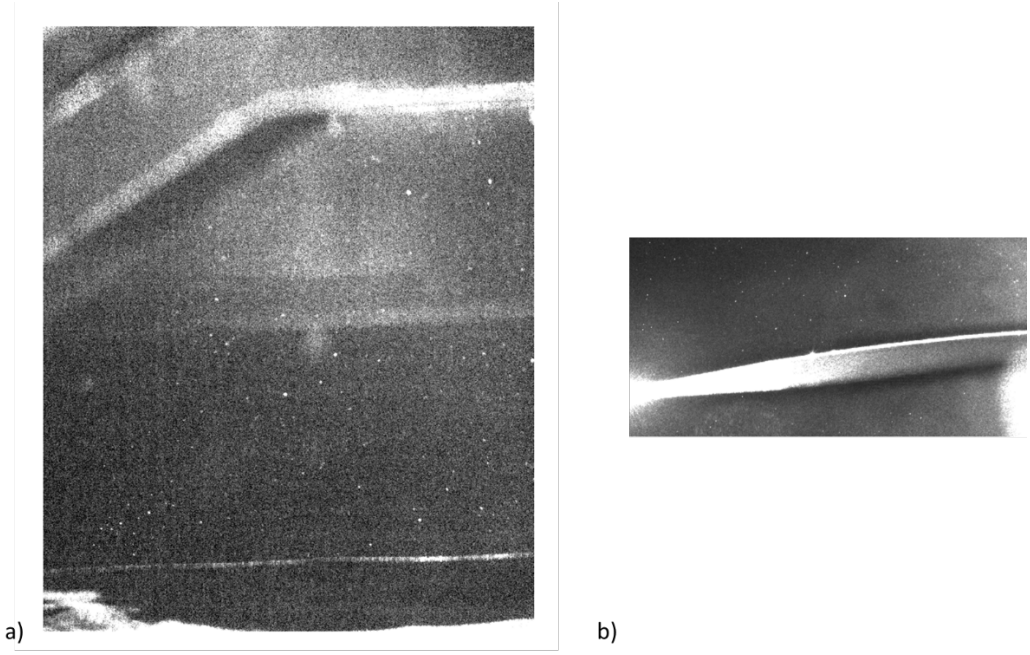

Figure 4. Sample raw data from both phases of testing. a) phase-1 experiments and b) phase-2 experiments.

III. Results and Discussion

This section presents and discusses the principal results from both the phase-1 and phase-2 studies described above. A detailed accounting of the data analysis methods used to obtain these results is presented in the appendix of this paper.

A. Phase 1 – Normal Shock

The phase-1 studies evolved significantly from the originally planned experiments. The broad goal of generating a stable, normal shockwave in a location that could be viewed through the limited optical access of the 0.3-m TCT facility was the only specification. The semi-span airfoil described in Section II.B above was the primary focus at first, since the presence of a shockwave had been inferred from previous testing [16]. However, the strength and spatial extent of the shockwave were completely unknown. Fortuitously, a new schlieren-type measurement system known as self-aligning, focused schlieren (SAFS) was looking for practical demonstrations of its capabilities, and a prototype of the SAFS system was installed in the 0.3-m TCT facility. The specifics of those experiments and the major outcomes are summarized in a companion paper to the current paper by Weisberger et al. [17]. Of particular interest to the phase-1 studies of this testing campaign was a series of experiments wherein different test articles were evaluated for their ability to generate a normal shockwave as well as some indication of the strength and spatial extent. The semi-span airfoil did in fact produce a shockwave, but its position oscillated and spatially did not appear to extend far enough into the viewable areas of the wind tunnel to be of practical utility. Additionally, partial-span (3/4) cylinder models were evaluated but were found unsuitable due both to the instability of the shockwaves formed in their wake and also the strength, which amounted to little more than Mach waves at the attainable tunnel operating conditions. It was only after those tests that the full-span supercritical airfoil (Fig. 1a) was evaluated; it was found to have stable shockwaves at a range of different tunnel operating conditions and model orientations, which were noted and used when the phase-1 studies commenced. The best results (i.e., strongest, most stable shockwave within the achievable field of view) were found to occur at a tunnel freestream Mach number of 0.74 with the AoA at 4°. A stronger shockwave was observed at higher AoAs but was ultimately too positionally unstable to used for the intended purpose.

The ensemble-averaged velocity field for the main test condition is shown in Fig. 5. These velocity data were acquired at a freestream Mach number of 0.74, total temperature of 200 K, and a 4° AoA. The normal shock is clearly visualized as the rapid decrease in velocity near the left (upstream) side of the image, with pre- and post-shock velocities of approximately 310 and 240 m/s, respectively, corresponding to a local Mach number of 1.17. The ensemble shown in Fig. 5 was constructed using data from 10 laser bursts. Due to the elevated operating temperature and low signal-to-noise ratio of these data, very few particles were present and visible within each field, and consequently attaining instantaneous velocity fields was not feasible. When evaluating particle size, in addition to full spanwise averaging, several sub-sampling methods were employed to generate velocity profiles as described in Appendix A. The resulting streamwise velocity profiles are shown in Fig. 6, with the cumulatively integrated profile as the most prominent sample. Using these traces, the approximate particles size was evaluated using the particle-dynamics model by Loth [18] (corrected by Williams et al. [19]). The resulting particle size measurements are shown in Fig. 7, with results for both ice crystals (Fig. 7a) and LN2 droplets (Fig. 7b) shown due to the current ambiguity in the particle composition. These different particle materials result in different particle size determinations because they have different densities. For ice crystals, the mean (effective) particle diameter (d_p) was found to be 1.62 μm, ranging from 0.18 μm to 2.95 μm over all samples tested. As is visible in Fig. 6, the approximate shock position did spatially vary to some extent, leading to a positive bias in the measured particle size (larger particle diameter) for the more heavily integrated sample traces. The corresponding results assuming LN2 droplets were a larger mean diameter of 1.95 μm and range of 0.31 μm to 3.57 μm. Studies by Hall et al. [10] may serve as a point of comparison, which utilized an optical droplet sizing probe to assess the naturally-occurring particles in 0.3-m TCT. Those studies found the most probable particle diameter to be around 3 μm, likely composed of solidified oil droplets, while a large quantity of smaller seed particles around 0.5 μm in diameter was also present and thought to be condensed LN2. The particle size measurements made in the present studies certainly fall within this range. However, caution should be used in making direct comparisons with these historic data, since the solidified oil droplets were no longer present only a year after those tests were conducted [11], and the current composition of the particles is unknown.

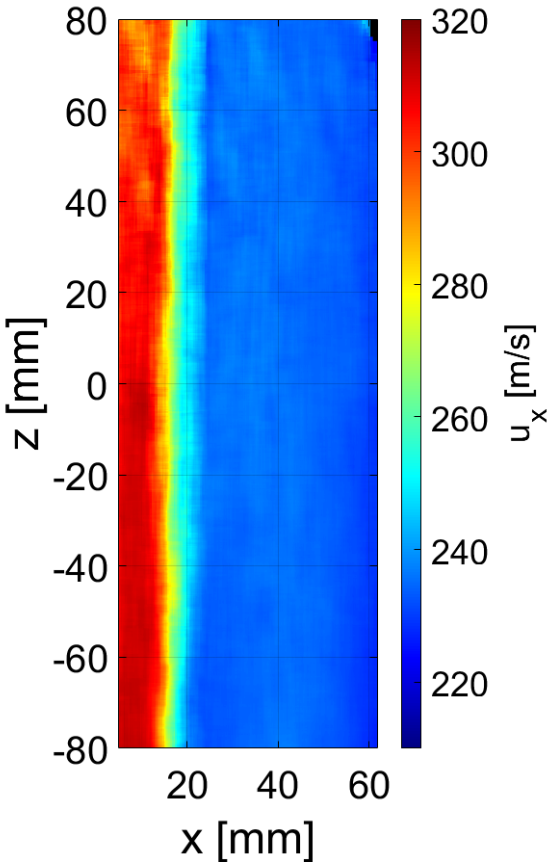

Figure 5. Ensemble-averaged velocity field from phase-1 studies. Test conditions were M∞ = 0.74, Pt = 192 kPa, Tt = 200 K, $\alpha = 4°$.

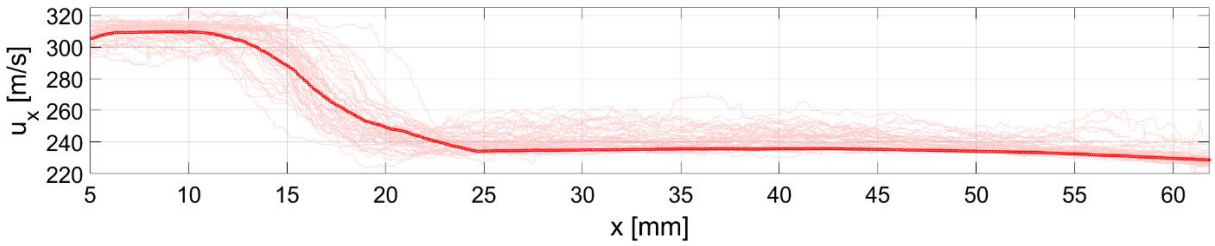

Figure 6. Partially- and fully-ensemble-averaged velocity profiles in airfoil flowfield demonstrating range of observed behaviors.

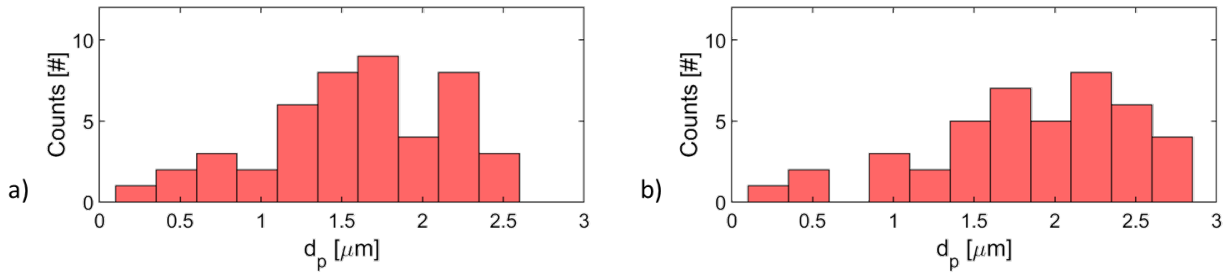

Figure 7. Distribution of measured particle size ensemble assuming a) water-ice crystals and b) liquid nitrogen droplets.

B. Phase-2 – High Lift

The phase-2 testing was intended as a secondary evaluation of the performance of naturally-occurring particles in the 0.3-m TCT. With an eye toward future high-lift testing in the NTF [20], where the detection of flow separation in high-lift test conditions is a needed measurement, simulating similar conditions and directly evaluating the performance of the particles in the 0.3-m TCT was a natural intermediate step and complementary to the phase-1 studies. The goals of these studies should be made clear at the outset of the discussion. First and foremost was the detection of flow separation. Flow separation using time-averaged PTV measurements would be obviated by either the direct observation of counter-motile particles in the raw data or nontangential flow over the airfoil in the processed velocity fields. Secondarily, the velocity measurements may themselves give some suggestion of excessive particle size, if not quantitatively, then at least as a fraction of the entire ensemble.

Toward the first goal of detecting flow separation, Fig. 8 depicts 3 representative raw streak images taken at different AoAs. The pathlines observed in the 8° case (Fig. 8a) indicate flow uniformly tangent to the airfoil surface at all locations, characteristic of fully attached flow. The 10° case (Fig. 8b) showed a small fraction of particles near the upper surface of the airfoil to be moving chaotically, intermittently vertical and/or against the principal flow direction. This effect grows in spatial extent and is observed to be happening continuously in the 12° case, though caution must be taken when interpreting these data due to the oblique orientation of the measurement plane. To contextualize these measurements more, Fig. 9 shows the orientation of the measurement plane with respect to the airfoil. Note that the velocity vectors point entirely in the x- and y-directions. Because of the way the measurement plane was viewed (normal to the x-direction) the observed motion can appear from the images to be in a purely x-y plane, when in fact there is a substantial variation in the spanwise position as well, covering over half the span of the airfoil model.

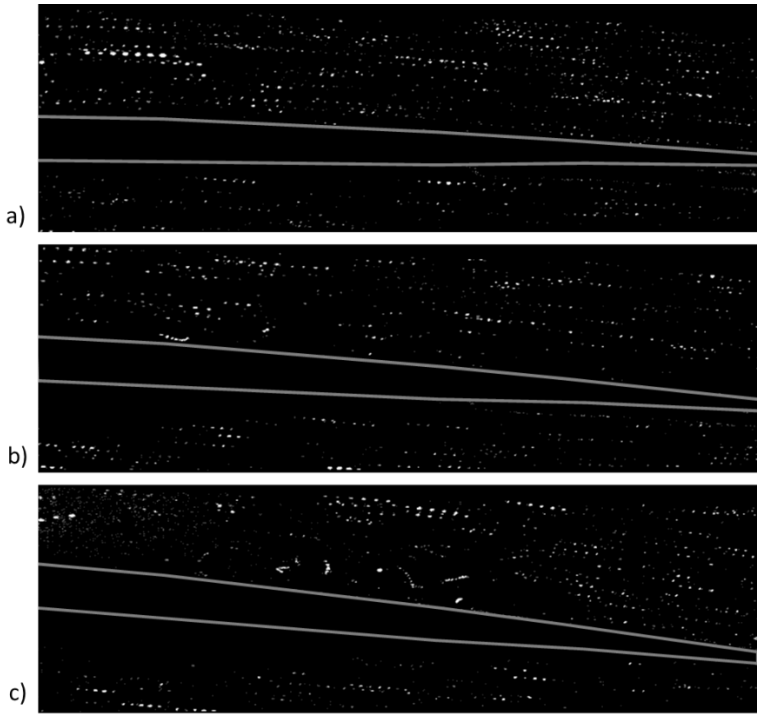

Figure 8. Sample streak images acquired at different angles of attack. a) α = 8°, b) α = 10°, and c) α = 12°. Flow is from left to right.

The ensemble/time-averaged velocity fields from four different AoAs are presented in Fig. 10, specifically 8°, 10°, 12°, and 13°; velocity profiles are shown for select streamwise/spanwise locations. The behaviors observed in these data echo the individual particle behaviors observed in Fig. 8. Specifically, fully attached flow is observed throughout the entire field of view in the 8° case (Fig. 10a). The velocity gradient associated with the increased angle of attack is also apparent on the underside of the airfoil. No appreciable velocity gradient was observed near the surface of the airfoil, likely indicating a boundary layer thinner than could be resolved with present detection system due to the amount

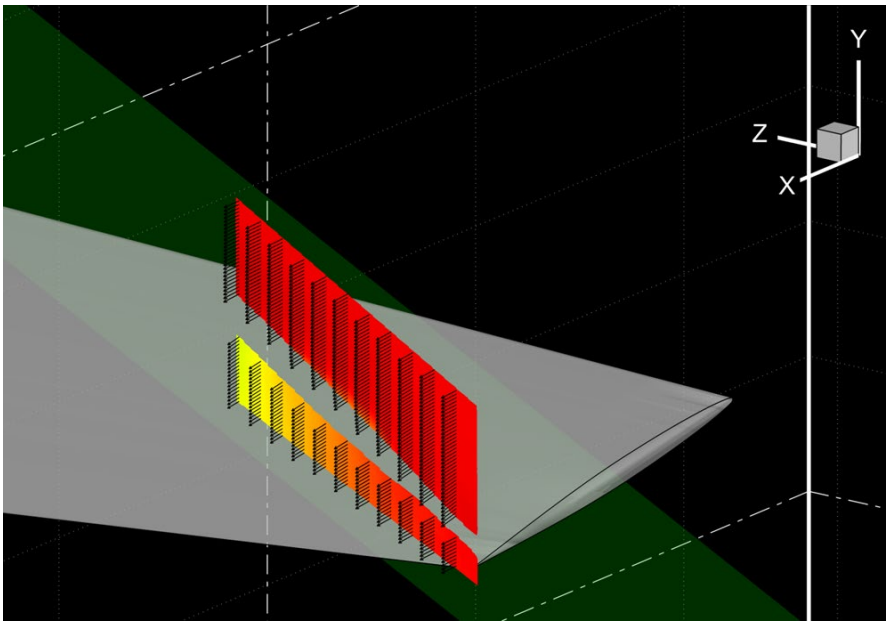

Figure 9. Perspective view of velocity field showing spatial orientation of vectors with respect to measurement plane and airfoil.

of laser flare that was present near the surface. For the 10° through 13° cases (Fig. 10b-d) a progressive growth of a low-velocity region on the upper surface is apparent. With regards to separated flow specifically, no separation was present in the mean of the 10° case. In contrast separated flow was present for both the 12° and 13° mean cases, made apparent by the lack of tangency of the local velocity vectors with respect to the airfoil surface. The 13° case exhibited a greater streamwise and spanwise extent to the separated flow region than the 12°. Velocity distributions within the regions of separated flow are shown in Fig. 11 for all cases. Measured velocities for the 8° case (Fig. 11a) are clustered in one primary group for both the streamwise and transverse velocities, consistent with the fully attached flow observed in the velocity fields. The 10° case (Fig. 11b) further confirms the observations made in the raw data (Fig. 8b) and mean velocity (Fig. 10b), wherein most of the particle velocities remain at or near the local mean velocity, while a few (<10 percent) deviate or move against the principal flow direction. Contrasting behaviors were observed for the 12° and 13° degree cases (Figs. 11c and 11d, respectively), in which many of the particles were nearly stagnant, with a small fraction of particles exhibiting velocities above freestream values. While not definitively a result of high particle inertia, the presence of high-velocity particles within a region of otherwise stagnant flow is one potential indicator of a larger particle size. A coarse estimate based on these plots would suggest 5-7 percent of the observed particle traces were too large to follow the flow within these regions.

C. Discussion

The measurements presented in Sections III.A and III.B represent a positive step toward understanding the behavior of the naturally-occurring particles within the 0.3-m TCT facility. First, it is worth noting the important synergy between these experiments and those of the companion paper by Weisberger et al. [17]. The ability to perform an *a priori* assessment of the flow using the SAFS system ensured that a relevant test environment for PTV was available for the Phase-1 studies. Ideally, the particle response assessment performed in the Phase-1 studies would have utilized full, instantaneous velocity fields generated using PIV. Numerous factors worked against this goal during testing. First, the limited optical access (single window for laser and camera transmission) made the experimental setup quite complex and necessitated both highly oblique viewing of the measurement plane and the observation of nearly pure backscatter. The scattering intensity was so low that the forward scattering from the back-reflection of the laser off the second window was of similar intensity to the incident laser beam. Second, condensation was observed on the windows at total temperatures below 200 K. Historically, the particle load within the test section had increased substantially below this temperature, meaning that the tests were conducted at suboptimal conditions. These two factors lead to data that had a very low signal-to-noise-ratio (SNR), and the (observable) particle density was insufficient to perform PIV. The alternative use of ensemble-averaged PTV for this purpose has its shortcomings, notably that the traces inherently incorporate shock unsteadiness into the velocity decay following the shockwave. Sub-sampling the data in time or space to generate the velocity traces improves this biasing to some extent but is not

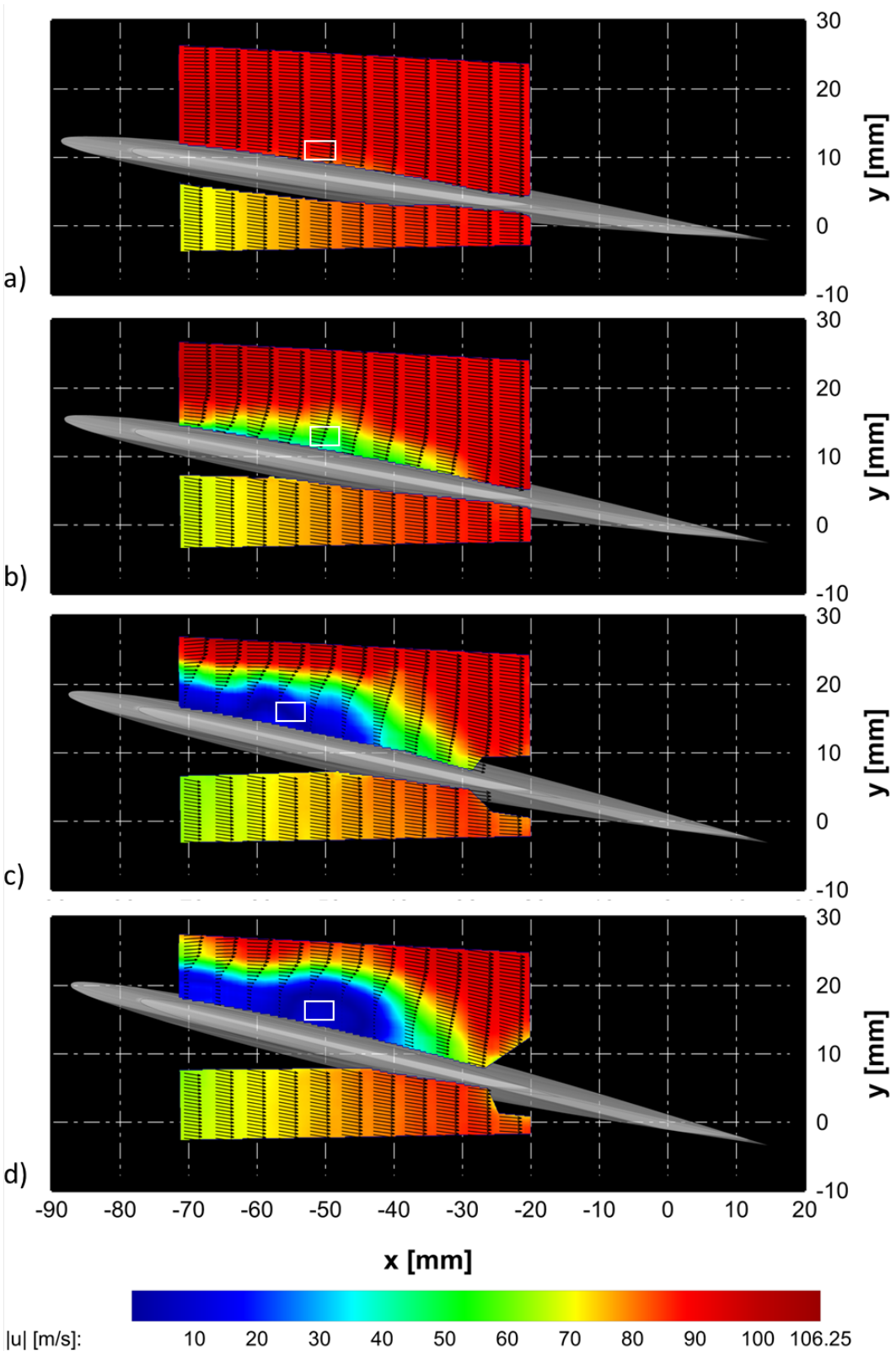

Figure 10. Ensemble-averaged velocity fields at different angles of attack under high-lift operating conditions. a) α = 8°, b) α = 10°, c) α = 12°, and d) α = 13°. Tunnel operating conditions were M_∞ = 0.25, Pt = 124 kPa, and Tt = 200 K. White boxes indicate regions sampled for generating Fig. 11.

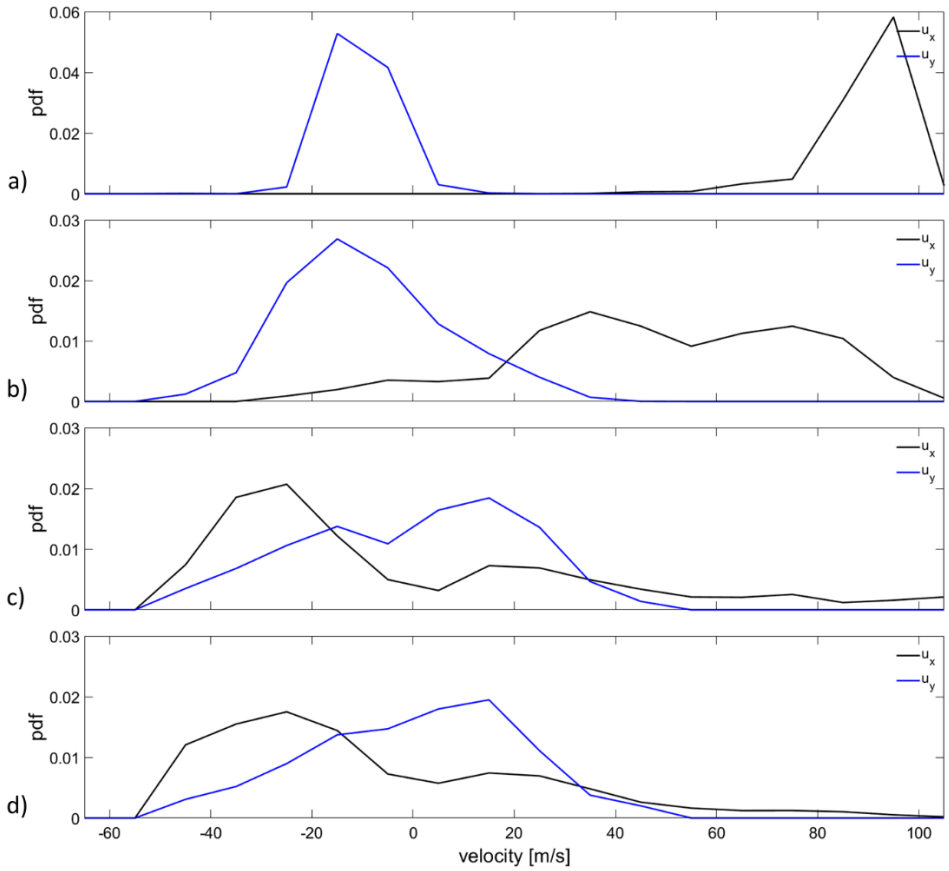

Figure 11. Velocity PDFs in separated flow regions for different AoAs. a) 8° case, b) 10° case, c) 12° case, and d) 13° case.

a true alternative to instantaneous data. Due to this motion, the measured particle diameters will always be biased toward a larger size.

In addition to the particle size measurements that have been presented in this section, these tests served to establish a framework through which similar assessments could be made in other facilities. It is unlikely that composition and character of the naturally-occurring particles found in 0.3-m would be the same as that in different wind tunnels. Studies in the NTF, for example, have noted that a fraction of their particles are likely fibers from insulation that pervaded the flow circuit [6]. For this reason, it is important and necessary to evaluate the particles using any of the methods described in this paper or other optical particle sizing techniques (which have not historically been successful in the 0.3-m facility). Particle-based measurements have recently been given greater consideration at the NASA TCT facilities. This consideration is in part due to the inconsistent nature of the FLEET technique that has been used to date [1,3]. FLEET was very effective in the 0.3-m TCT facility during the initial testing runs [2,16] but experienced operational issues when implemented in the NTF, particularly at the lowest operating temperatures. These issues were largely the result of the longer distances over which the technique had to operate (inhibiting focal stability of the laser), coupled with unceasing experimental difficulties resulting from the complex camera and laser penetration systems being immersed in the cryogenic environment. To date, FLEET has never been fully operational at full cryogenic conditions at the NTF. Consequently, interest in particle-based measurements has risen due to the presence of particles over much of the operational envelope of the facilities. Combined with simplified laser transmission and image acquisition, particle-based measurements using naturally-occurring particles may become the norm for velocity measurements if a sufficiently robust means of characterizing the particles can be enacted.

IV. Conclusions

A series of tests was conducted with the intent of assessing the aerodynamic character of the naturally-occurring particles in the NASA Langley 0.3-m TCT facility. PTV was used to measure the velocity lag of particles traversing

a normal shock generated by a supercritical airfoil. For the selected conditions, particles ranging in size from 0.18 to 3.57 μm were observed, with the mean particle size measuring between 1.62 to 1.95 μm. The response of particles to separated flow was evaluated by performing PTV on the flowfield around a semi-span airfoil model at high-lift tunnel operating conditions. The resulting raw data and processed velocity fields indicated a transition from fully-attached to fully-separated flow over the upper surface of the airfoil with increasing angle of attack. The assessment of the measured velocity distributions within these regions suggested less than 10 percent of the particles were too large to respond to the separation of the flow. While the results from these tests were encouraging, they were ultimately specialized to the 0.3-m facility, and similar assessments would be required in any facility attempting to utilize naturally-occurring particles. With the increased interest in particle-based measurements in TCT facilities, making more robust measurements of this type and improving surrounding technologies such as laser transmission would improve the outlook of these techniques going forward.

V. Appendix

A. Data analysis

This appendix discusses all elements of the data analysis used in the processing of the raw data from both phases of the test. All processing was done with in-house developed codes.

1. Image processing

The data from both phases of testing underwent the same basic preprocessing steps. First, the raw data was dewarped/corrected for perspective distortions. This procedure was achieved using a third-order polynomial fit to the points on a calibration target (dotcard). Following dewarping, the data were cropped as necessary (only for the phase-1 studies). Then, a global intensity normalization was performed on the data to correct for laser intensity variations across each burst of data. A small area of each image outside of the active region of interest was selected and monitored for intensity variations shot-to-shot, and an overall correction was applied to equalize the intensity image-to-image. Finally, a sliding background subtraction was performed by averaging over 5 images and subtracting the resulting image from the middle image of the set. This procedure was more effective than a standard background subtraction due to the significant burst-to-burst variation in laser beam profile.

2. Particle detection

The phase-1 and phase-2 studies utilized different algorithms for particle detection. The SNR in the phase-1 studies were very poor (of order unity). To get around this issue, a progressive image threshold was performed in which the images were converted to binary images with progressively higher thresholds (generally from 5 percent to 50 percent of saturation). At each stage of the threshold scan, the overall area of each contiguous area of the binary image encompassed by the particles was assessed. Since the particle images were all of a similar size, a potential particle was identified once an individual intensity object of that approximate size was detected. The subsequent steps in the threshold scan continued to locate more potential particles, with objects in nearly the same location identified with each other. Once this threshold sweep was completed for an image pair, approximate particle locations were identified by taking an intensity weighted centroid over the determined area. Then as a pre-filtering step, estimated particle displacements were used to identify potential particle pairs. For each detected particle in the first frame of data, all potential objects within the second frame were scanned to find the closest match to the estimated displacement. If none existed within a specified tolerance (10 pixels usually), the particle was considered false. Once the list of potential particles was fully identified, a bivariate Gaussian profile was fit to each potential particle in the image, allowing sub-pixel location determination. This step was done to prevent peak-locking in the final velocity results.

The phase-2 data was of considerably higher SNR and was amenable to standard PTV detection schemes. For these data, the core of the Part2Track PTV engine [21] was utilized to identify particle locations.

3. Displacement and velocity determination

The double-frame PTV data from the phase-1 studies were subjected to 2 basic filters when determining the validity of a particle pair. The particle pairs identified in the previous step were reaffirmed once the sub-pixel location scheme was completed in the previous processing step. These estimated displacements (in both the x- and z-directions) were then subject to local and global min/max displacement filters to remove significant outliers from the datasets. A local RMS filter was applied to nearby particle pairs to remove significant local outliers. Particle pairs that remained after these steps were tagged with metadata containing information about the partition and image from which they originated. Peak locking was not observed significantly in these data; a histogram of the sub-pixel particle

displacements can be seen in Fig. A.1a. No appreciable focus existed around 0 px, which would be indicative of peak locking. Velocities were calculated based on the scale of the dewarped data and the time step between the images, which was 2.5 or 5 μs for most of these data.

Phase-2 PTV data were a time-series, and thus longer trajectories could be constructed when evaluating velocities. The Part2Track engine was again used for this purpose. Constructed trajectories typically reached a maximum length of 5 or 6 images before losing correlation strength; particles within the 'freestream' areas of the flow were the exception due to their simple shapes. Trajectories containing only 2 points were discarded (representing only 3 percent of the measured trajectories). As with the phase-1 data, min/max velocity filters and RMS local outlier filters were applied to the data to remove extraneous trajectories. Finally, because of the significant variation in magnification that existed throughout the image, a correction was applied. This correction used the first image in each trajectory to determine the approximate spanwise position of the particle, and then a multiplicative factor was applied to each trajectory to account for variations from the mean magnification. As with the phase-1 studies, no significant peak locking was detected in the data (see Fig. A.1b). Velocities were calculated as the mean across each measured trajectory.

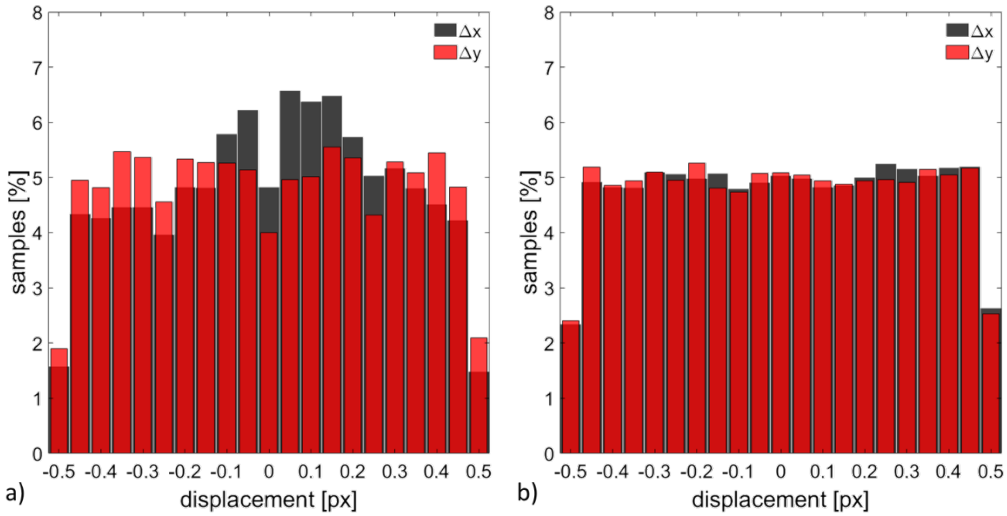

Figure A.1. Histograms of sub-pixel particle displacements. a) phase-1 studies and b) phase-2 studies. No significant peak locking was observed in either phase of testing.

4. Velocity field construction

The primary velocity trace for the phase-1 studies were constructed by integrating all data points in the spanwise (z-) direction. To do this, the streamwise integration windows 32 px in width (with 31-px overlap) were used to collect data. While excessively wide in the baseline case, this width was chosen to provide a sufficient number of samples at the highest degree of sub-sampling. Sub-sampling the data was done in three specific ways: 1) streamwise slicing of the cumulative dataset, 2) single-partition data fully integrated in the spanwise direction, and 3) single-partition data with streamwise slicing. Overall, 55 trajectories were extracted from the dataset in this manner. A homologous process was used to construct the 2-dimensional velocity fields in the phase-2 data. The region of interest was subdivided into bins 16 px × 16 px (with 15-px overlap to improve the appearance, though it has no effect on the spatial resolution). Trajectory centers were located within each integration window, and velocities were averaged to generate the velocity fields.

5. Particle diameter fitting

The phase-1 data utilized a least-squares optimization routine to determine the best match of particle size to each velocity profile. At the core of this optimization scheme was a particle dynamics solver based on the work of Loth [18] (with the correction to one of the terms made by Williams [19]). The solver utilized a forward-Euler scheme for time evolution (using a time step of 10 ns). At each time step, the particle position and velocity were evaluated and used as inputs to the next time step. Particle positions were evolved over a fixed spatial domain encompassing a short region upstream and downstream of the approximate shock location. After the particle dynamics simulations completed, a spatial averaging filter was applied that matched the integration windows used in constructing the

velocity profiles. The optimization scheme repeatedly evaluated particle diameters and shock locations until exit criteria were met, specifically a residual tolerance of 10^{-5}. Particle diameters and shock positions were recorded for use in later statistical assessments.

Acknowledgments

The authors would like to thank all of the expert staff at The NASA Langley Research Center's 0.3-m TCT including (but not limited to) Michael Chambers, Cliff Obara, Reggie Brown, Gary Beachem, and Harry Stotler. These tests would not have been possible without the long hours and hard work everyone contributed. The contributions of Josh Weisberger, Matthew Boyda, and Brett Bathel and their SAFS system were invaluable to the completion of these tests. Additional thanks are given to Jon Retter for his previous contributions to this project. This work was funded by NASA's Transformational Tools and Technologies (TTT) program, Innovative Measurements (IM) discipline under the leadership of Mark Wernet (The NASA Glenn Researcher Center) and with input from Lee Mears and Melissa Rivers (The NASA Langley Research Center).

References

[1] Reese, D.T., Burns, R.A., Danehy, P.M., Walker, E.L., Goad, W.K., "Implementation of a pulsed-laser measurement system in the national transonic facility," *AIAA Aviation Forum 2019*, Dallas, TX, 2019.

[2] Burns, R.A., Danehy, P.M., Halls, B.R., and Jiang, N., "Femtosecond laser electronic excitation tagging velocimetry in a transonic cryogenic wind tunnel," *AIAA Journal*, Vol. 55, No. 2, 2017, pp. 680-685.

[3] Reese, D.T., Thompson, R.J., Burns, R.A., and Danehy, P.M., "Application of femtosecond-laser tagging for unseeded velocimetry in a large-scale transonic cryogenic tunnel," *Experiments in Fluids*, Vol. 62, No. 99, 2021.

[4] Konrath, R., Otter, D., Geisler, R., Agocs, J., Mattner, H., Roosenboom, E.W.M., Fey, U., Quest, J., and Kuehn, C., "Adaptation of PIV for Application in Cryogenic Pressurized Wind Tunnel Facilities at High Reynolds Numbers," *15th International Symposium on Application of Laser Techniques to Fluid Mechanics*, Lisbon, Portugal, 2010.

[5] Hall, R.M. "Onset of Condensation Effects with an NACA 0012-64 Airfoil Tested in the Langley 0.3-Meter Transonic Cryogenic Tunnel." *NASA Technical Paper 1385*, 1979.

[6] Herring, G.C., Lee, J.W., and Goad, W.K., "Feasibility of Rayleigh Scattering Flow Diagnostics in the National Transonic Facility," NASA TM-2015-218800, 2015.

[7] Gartrell, L.R., Gooderum, P.B., Hunter Jr., W.W., and Meyers, J.F. "Laser Velocimetry Technique Applied to the Langley 0.3-Meter Transonic Cryogenic Tunnel." *NASA Technical Memorandum 81913*, 1981.

[8] Honaker, W. C. "Velocity and Flow Angle Measurements in the Langley 0.3-Meter Transonic Cryogenic Tunnel Using a Laser Transit Anemometer." *NASA-CP2243*, 1982.

[9] Retter, J.E., Burns, R.A., Fisher, J.M., Felver, J.J., Reese, D.T., and Danehy, P.M., "On the use of liquid nitrogen droplets as flow tracers in cryogenic flow facilities at NASA Langley Research Center," *AIAA SciTech Forum 2021*, Virtual Event.

[10] Hall, R.M. Pre-Existing Seed Particles and the Onset of Condensation in Cryogenic Wind Tunnels. *AIAA 22nd Aerospace Sciences Meeting*, 1984.

[11] Honaker, W.C., and Lawing, P.L. “Measurements in the Flow Field of a Cylinder with a Laser Transit Anemometer and a Drag Rake in the Langley 0.3 M Transonic Cryogenic Tunnel.” *NASA Technical Memorandum 86399*, 1985.

[12] Singh, J.J., Marple, C.G., and Davis, W.T. “Characterization of Particles in the Langley 0.3-Meter Transonic Cryogenic Tunnel Using Hot Wire Anemometry.” *NASA Technical Memorandum 84551*, 1982

[13] Qi, Y., Ye, H., and Hu, Q., “Mechanisms of trace water vapor desublimation over airfoil in transonic cryogenic wind tunnels,” *Physics of Fluids*, Vol. 34, 2022.

[14] Johnson, W.G., Hill, A.S., and Eichman, O., “High Reynolds Number Tests of a NASA SC(3)-0712(B) Airfoil in he Langley 0.3-Meter Transonic Cryogeinc Tunnel,” *NASA-TM-86371*, 1985.

[15] Watkins, A.N., Leighty, B.D., Lipford, W.E., Goodman, K.Z., “Pressure- and Temperature-Sensitive Paint at 0.3-m Transonic Cryogenic Tunnel,” *NASA-TM-2015-218801*, 2015.

[16] Burns, R.A., Danehy, P.M., “Unseeded velocity measurements around a transonic airfoil using femtosecond laser tagging,” *AIAA Journal*, Vol. 55, No. 12, 2017.

[17] Weisberger, J.M., Bathel, B.F., Danehy, P.M., Boyda, M.T., Tyrrell, O.K., Ripley, W.H., Jones, G.S., Burns, R.A., Kwok, A.K., and Jones, S.B., “Self-Aligned Focsing Schlieren at the 0.3m Transonic Cryogenic Tunnel and the National Transonic Facility,” *AIAA Scitech Forum 2024*, Orlando, Fl, USA.

[18] Loth, E., “Compressibility and Rarefaction Effects on Drag of a Spherical Particle,” *AIAA Journal*, Vol. 46, No. 9, 2008.

[19] Williams, O.J.H., Nguyen, T., Schreyer, A.M., and Smits, A.J., “Particle response analysis for particle image velocimetry in supersonic flows,” *Physics of Fluids*, Vol. 27, 2015.

[20] Clark, A.M., Slotnick, J.P., Taylor, N.J., and Rumsey, C.L., “Requirements and Challenges for CFD Validation within the High Lift Common Research Model Ecosystem,” *AIAA Aviation 2020 Forum*, Virtual Event.

[21] Janke, T., Schwarze, R., and Bauer, K., “Part2Track: A MATLAB package for double frame and time resolved Particle Tracking Velocimetry,” *SoftwareX*, Vol. 11, 2020.